Evaluation of a Nonlocal Quasi-Phase Observation Operator in Assimilation of CHAMP Radio Occultation Refractivity with WRF

HUI LIU, JEFFREY ANDERSON, YING-HWA KUO, CHRIS SNYDER, AND ALAIN CAYA

National Center for Atmospheric Research, Boulder, Colorado

(Manuscript received 3 October 2006, in final form 18 April 2007)

ABSTRACT

A nonlocal quasi-phase radio occultation (RO) observation operator is evaluated in the assimilation of Challenging Minisatellite Payload (CHAMP) radio occultation refractivity using a Weather Research and Forecasting (WRF) ensemble data assimilation system at 50-km resolution. The nonlocal operator calculates the quasi phase through integration of the model refractivity along the observed ray paths. As a comparison, a local refractivity operator that calculates the model refractivity at the observed ray perigee points is also evaluated. The assimilation is done over North America during January 2003 in two different situations: in conjunction with dense, high-quality radiosonde observations and with only satellite cloud drift wind observations. Analyses of temperature and water vapor with the RO refractivity assimilated using the local and nonlocal operator are verified against nearby withheld radiosonde observations. The bias and RMS errors of the analyses of water vapor and temperature using the nonlocal operator are significantly reduced compared with those using the local operator in the troposphere when the only additional observations are satellite cloud drift winds. The reduction of the bias and RMS errors is reduced when radiosonde observations are assimilated.

1. Introduction

Atmospheric limb sounding making use of signals transmitted by the global positioning system (GPS) has evolved as a promising global observing system. By placing GPS receivers onboard low-earth-orbiting satellites, one can measure the delays of radio signals transmitted by GPS satellites due to the refractivity structure of the earth's atmosphere as they set or rise behind the earth (Ware et al. 1996; Kursinski et al. 1997). The delays of the signal are integrated effects of the atmospheric refractivity along the ray paths of the signals, which usually extend several hundred kilometers in the troposphere (Kursinski et al. 1997). From the measurements, one can derive vertical profiles of bending angles and refractivity using the Abel inversion under the assumption of local spherical symmetry. Details of the GPS data retrieval process conducted at the University Cooperation for Atmospheric Research (UCAR) can be found in Kuo et al. (2004).

The bending angle and refractivity profiles can be used to reduce the errors of temperature and water vapor of the first guess/forecasts through assimilation with numerical weather and climate models. An observation operator, which calculates the bending angle or refractivity from the model state variables, is required. A "local" operator uses temperature, water vapor, and pressure at the estimated tangent points of the radio rays to calculate the bending angles or refractivity. A nonlocal operator takes account of the variations of the temperature, water vapor, and pressure along the ray paths.

When there exist strong horizontal gradients of atmospheric refractivity in the middle and lower troposphere, forward modeling of radio occultation (RO) refractivity/bending angle using local operators may have significant errors. Use of nonlocal operators may significantly reduce the forward modeling errors (see, e.g., Sokolovskiy et al. 2005a,b; Syndergaard et al. 2005, 2006; Poli 2004; Foelsche and Kirchengast 2004). For example, Sokolovskiy et al. (2005a) showed that use of a nonlocal quasi-phase operator may reduce the forward modeling errors using the Weather Research and Forecasting (WRF) model, especially in the middle and lower troposphere in a few cases of strong horizontal gradient of refractivity, compared with use of a local

Corresponding author address: Hui Liu, 1850 Table Mesa Dr., Boulder, CO 80305.
E-mail: hliu@ucar.edu

DOI: 10.1175/2007MWR2042.1

operator. The error reduction using the nonlocal operator is more significant at horizontal model resolutions of 100 km or less. At resolutions of 200 km or coarser, the use of the nonlocal operator does not have an obvious positive impact and the use of a local operator may have sufficient accuracy.

A number of nonlocal and local refractivity/bending angle operators have been tested in assimilation of GPS radio occultation data with global and regional data assimilation systems (Healy and Thepaut 2006a; Healy et al. 2006b; Zou et al. 1999; Kuo et al. 2000; Liu and Zou 2003). The benefit of using nonlocal operators, however, has not been demonstrated in the troposphere with high-horizontal-resolution data assimilation systems (<100 km).

In this study, the impact of using the nonlocal quasi-phase operator in assimilation of Challenging Minisatellite Payload (CHAMP) RO refractivity with a relatively high-horizontal-resolution (50 km) version of the WRF model is examined focusing on the middle and lower troposphere. The ensemble adjustment Kalman filter (EAKF; Anderson 2001, 2003) is used to assimilate the refractivity with the WRF model because of the easy implementation of the observation operators and use of flow-dependent forecast error covariances to model the first guess/forecast errors.

In section 2, the WRF ensemble data assimilation system is briefly introduced. The implementation of the nonlocal quasi-phase operator with the WRF ensemble data assimilation system is described in section 3. The experimental design for examining the performance of the nonlocal operator is given in section 4. The CHAMP RO refractivity and satellite cloud drift wind data are described in section 5. The latitudinal distribution of the horizontal gradients of refractivity of the WRF forecasts in the troposphere and the departures of the first guess calculated using the nonlocal and local operator from the observations are discussed in sections 6 and 7, respectively. Evaluation of the nonlocal operator is presented in sections 8 and 9. Conclusions and discussion are presented in section 10.

2. WRF ensemble data assimilation system

The WRF ensemble data assimilation system uses the Data Assimilation Research Testbed (DART) of the National Center for Atmospheric Research (NCAR). The EAKF is used to assimilate observations with WRF short-range forecasts as first guess. A brief description of the EAKF is given in the following. Assuming observational error distributions of the observations are independent for each scalar observation, the observations can be assimilated sequentially in any order by the EAKF. Here, we describe only how the EAKF works for assimilation of a single observation, y^o.

A joint state–observation vector is defined as

$$\mathbf{z} = [\mathbf{x}, H(\mathbf{x})] = [\mathbf{x}, \mathbf{y}], \tag{2.1}$$

where $\mathbf{x}$ is the model state variable vector; $\mathbf{y} = H(\mathbf{x})$ is the prior estimate (first guess) of the observation given x obtained by applying the forward observation operator H to the model state.

Using Bayesian statistics, the updated (analyzed or posterior) probability distribution, $\mathbf{z}^u = [\mathbf{x}^u, \mathbf{y}^u]$, can be computed from the prior probability distribution, $\mathbf{z}^p = [\mathbf{x}^p, \mathbf{y}^p]$, as

$$p(\mathbf{z}^u) = p(y^o|\mathbf{z}^p)p(\mathbf{z}^p)/\text{normalization}, \tag{2.2}$$

where y^o is the single observation. A prior ensemble of the model state variables, $\mathbf{x}_i^p$ ($i = 1, \ldots, K$), can be obtained from an ensemble integration of the model to the time when the observation is available, where i is the index of the ensemble member and K is the ensemble size. A prior ensemble estimate of the observation, $\mathbf{y}_i^p$ ($i = 1, \ldots, K$), can be obtained by applying the forward observation operator H to each ensemble member, $\mathbf{x}_i^p$.

The updated probability for the marginal distribution of y can be formed as

$$p_y(\mathbf{y}^u) = p(y^o|\mathbf{y}^p)p_y(\mathbf{y}^p)/\text{normalization}. \tag{2.3}$$

The assimilation of the observation can be done in two steps. The first step determines updated estimates of the ensemble members, $\mathbf{y}_i^u$ ($i = 1, \ldots, K$), for the observation using the ensemble adjustment method and computes increments between the prior and updated ensemble estimates of the observation. The second step determines the updated ensemble of the model state variables, $\mathbf{x}_i^u$ ($i = 1, \ldots, K$), from these observation space increments. In practice, the following procedures are involved:

1) Generate a prior ensemble, $\mathbf{x}_i^p$ ($i = 1, \ldots, K$), at the time when the observation is available.
2) Get a prior ensemble estimate of the observation, $\mathbf{y}_i^p$ ($i = 1, \ldots, K$), by applying the forward observation operator to each member of the prior ensemble,

$$\mathbf{y}_i^p = H(\mathbf{x}_i^p), \quad i = 1, \ldots, K. \tag{2.4}$$

3) Compute the prior ensemble mean $\overline{\mathbf{y}^p}$ and variance Σ^p:

$$\overline{\mathbf{y}^p} = \frac{1}{K}\sum_{i=1}^{K} \mathbf{y}_i^p, \tag{2.5}$$

$$\Sigma^p = \frac{1}{K-1}\sum_{i=1}^{K} (\mathbf{y}_i^p - \overline{\mathbf{y}^p})(\mathbf{y}_i^p - \overline{\mathbf{y}^p}). \tag{2.6}$$

4) Compute the updated/analysis variance and mean of the ensemble in observation space as follows:

$$\Sigma^u = [(\Sigma^P)^{-1} + (\Sigma^o)^{-1}]^{-1}, \quad (2.7)$$

$$\overline{\mathbf{y}^u} = \Sigma^u(\overline{\mathbf{y}^p}/\Sigma^p + y^o/\Sigma^o), \quad (2.8)$$

where Σ^o is the so-called observation error variance, which may include observation measurement errors and the model's representative errors of the observation. In other words, the updated ensemble mean is shifted closer to the observed value and the variance of the updated ensemble of the observation is reduced due to the combination of the information from the observation.

5) Get the updated ensemble members by shifting the mean and linearly contracting the deviation of the ensemble members about the prior ensemble mean:

$$\mathbf{y}_i^u = (\mathbf{y}_i^p - \overline{\mathbf{y}^p})\sqrt{\Sigma^u/\Sigma^p} + \overline{\mathbf{y}^u}, \quad i = 1, \ldots, K. \quad (2.9)$$

In this way, the updated mean and variance of the ensemble of the observation are exactly $\overline{\mathbf{y}^u}$ and Σ^u. The increment for each ensemble member of the observation can be obtained by $\Delta\mathbf{y}_i = \mathbf{y}_i^u - \mathbf{y}_i^p$.

6) Compute the prior ensemble variance of the observation ($\sigma_{y,y}^p$) and the prior covariance ($\sigma_{x_j,y}^p$) of $\mathbf{y}^p$ with each model state variable, $\mathbf{x}_j^p$, which is to be updated. Here, j is the index of model state variables and

$$\sigma_{y,y}^p = \frac{1}{K-1}\sum_{i=1}^{K}(\mathbf{y}_i^p - \overline{\mathbf{y}^p})(\mathbf{y}_i^p - \overline{\mathbf{y}^p})^{\mathrm{T}}, \quad (2.10)$$

$$\sigma_{x_j,y}^p = \frac{1}{K-1}\sum_{i=1}^{K}(\mathbf{x}_{i,j}^p - \overline{\mathbf{x}_j^p})(\mathbf{y}_i^p - \overline{\mathbf{y}^p})^{\mathrm{T}}, \quad (2.11)$$

where

$$\overline{\mathbf{x}_j^p} = \frac{1}{K}\sum_{i=1}^{K}\mathbf{x}_{i,j}^p. \quad (2.12)$$

7) Assuming the prior error distribution of the model state variables is Gaussian, the corrections to the prior of the model variables can be obtained from the increments to the prior ensemble of the observation ($\Delta\mathbf{y}_i$) by a linear regression:

$$\Delta\mathbf{x}_{j,i} = \frac{\sigma_{x_j,y}}{\sigma_{y,y}}\Delta\mathbf{y}_i, \quad i = 1, \ldots, K; \quad j = 1, \ldots, M, \quad (2.13)$$

where M is the number of model state variables. As shown in Anderson (2003), the state variables can be updated sequentially given the observation increments $\Delta\mathbf{y}_i$.

8) The updated ensemble is

$$\mathbf{x}_{j,i}^u = \mathbf{x}_{j,i}^p + \Delta\mathbf{x}_{j,i}, \quad i = 1, \ldots, K; \quad j = 1, \ldots, M. \quad (2.14)$$

It can be seen that the corrections to the model state variables are proportional to the covariance between the prior ensemble estimate of the observation and the prior ensemble of the model variables.

To reduce the noise in the sample covariance estimates for observations with physically remote model state variables in (2.11), especially when a small ensemble size is used, a horizontal distance dependent factor {the Gaspari–Cohn fifth-order polynomial [Gaspari and Cohn 1999, their Eq. (4.10)]} multiplies the forecast covariance $\sigma_{x_j,y}$. The half-width of the function used here is 650 km. When the distance between the observation and the state variable is larger than 1300 km, the impact of the observation goes to zero. This localization half-width distance is large enough to span the area of dependence of an RO refractivity observation, approximately 300–500 km around the GPS RO observation perigee locations in the troposphere (Kursinski et al. 1997).

The current version of the WRF ensemble data assimilation system can assimilate radiosonde observations, aircraft reports, satellite winds, retrieved temperature and water vapor profiles from satellite radiances, and many kinds of surface observations. GPS RO refractivity can also be assimilated using both local and nonlocal observation operators. In this study, WRF 6-h forecasts at 50-km horizontal resolution with 28 vertical levels from the surface to 50 hPa (~20-km altitude) are assimilated with CHAMP refractivity observations.

One advantage of using the ensemble data assimilation system is that various nonlocal RO observation operators can be implemented easily without the development of tangent linear and adjoint models. Another important advantage is that time-varying multivariate forecast error covariance of temperature with water vapor is included in the assimilation of RO data. The forecast error of water vapor may be correlated with that of temperature because of the dynamical and physical processes involved as well as the deficiencies of physical parameterizations in the forecast model (see, e.g., Liu et al. 2007). The forecast error covariances involving water vapor may also be highly time and space dependent. Using the information from the flow-dependent multivariate forecast error "covariance" for

temperature and water vapor should improve the correction of the forecast errors in temperature and water vapor. Our previous study shows that inclusion of these forecast error correlations in the ensemble data assimilation system significantly reduces the analyses errors of temperature and water vapor in the assimilation of idealized RO measurements (Liu et al. 2007).

3. Implementation of the nonlocal quasi-phase operator

The neutral atmospheric refractivity is defined as

$$N = (n - 1) \times 10^6 = 77.6 \times P/T + 3.73 \times 10^5 \times e/T^2,$$

where n is the refractive index, P is pressure (hPa), T is temperature (K), and e is water vapor partial pressure (hPa) (Kursinski et al. 1997).

For the local RO refractivity operator, the first guess of temperature, pressure, and water vapor on the WRF model grid is interpolated linearly in the vertical and horizontal directions to the RO observations' locations. The local refractivity is then calculated from the temperature, pressure, and water vapor.

For the nonlocal quasi-phase operator, a preprocessing step for observations is required that calculates observation quasi-excess phase using refractivity from radio occultation observations:

$$S_{\text{obs}} = \int_{\text{ray}} N_{\text{RO}}(r)\, dl, \tag{3.1}$$

where $r = r_c + z$, r_c is the local curvature radius of the earth, and z is the height above the earth's surface. The rays are approximated as straight lines starting from the observations' locations along the observed ray directions and stopping at 15 km above the earth's surface (a bit below the WRF model top at 20 km to avoid the impact of the damped upper boundary of the model).

The next equation presents the nonlocal quasi-phase operator that calculates quasi phase from the refractivity of the first guess, where the rays are the same as in the calculation of phase observations:

$$S_{\text{guess}} = \int_{\text{ray}} N_{\text{guess}}(x, y, z)\, dl. \tag{3.2}$$

A constant step size of 5 km (Sokolovskiy et al. 2005a) is used in the integrations of (3.1) and (3.2). In (3.1), the refractivity at an arbitrary point along the rays is calculated from the observation refractivity using a vertical linear interpolation. In (3.2), the first-guess refractivity at an arbitrary point along the rays is calculated from the first-guess refractivity field using linear interpolations in both vertical and horizontal directions.

The computational cost of the nonlocal operator along a single ray path at 10 and 2 km above surface is ~0.001 and 0.0018 s of CPU, respectively, on a Linux cluster of NCAR. The cost of the local one is ~0.000 01 s of CPU. The ratio of the cost of nonlocal to local operator is ~100 and ~160 at 10 and 2 km above the surface, respectively. The impact of the computational cost of the nonlocal operator, however, may be significantly reduced if all of other factors in the assimilation step are considered. For example, the ratio of assimilating using the nonlocal operator to local operator is 1.14 when one RO profile is assimilated with the WRF forecast given the fact that the ensemble assimilation system spends significant CPU time on initialization, input/output, etc.

4. Experimental design

In regions where conventional high-quality data (e.g., radiosondes) are sparse, like over the oceans, the impact of GPS RO data is expected to be larger than for conventional data-dense regions. This may be especially true in the presence of thick clouds over the oceans as in the case of winter storms or hurricanes. In the presence of thick precipitating clouds, satellite radiances can have larger uncertainties. In this study, we choose to evaluate the nonlocal operator in two different situations: in conjunction with dense radiosondes and with only satellite cloud drift wind observations. The latter situation serves as an upper bound on the impact of GPS data. Many additional observation data types not used here are in fact assimilated in operational global and regional data analyses systems.

Two sets of experiments are done. The first set includes the following:

- Experiment I: Assimilate only satellite cloud drift wind observations.
- Experiment II: Assimilate the same set of satellite wind observations as in experiment I plus RO refractivity using the nonlocal operator.
- Experiment III: Same as experiment II, but assimilate the RO refractivity using the local refractivity operator.

The second set includes the following:

- Experiment IV: Assimilate radiosonde observations including wind, temperature, and specific humidity. Radiosonde observations within 200 km and ±3 h of an RO observation are withheld for verification.

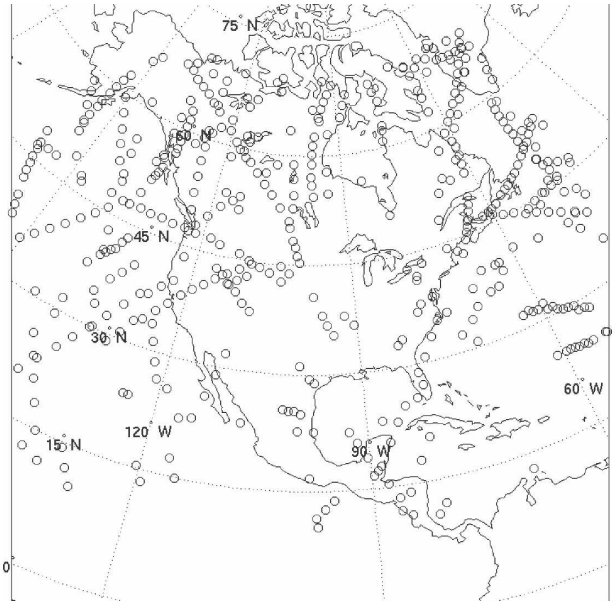

FIG. 1. Locations of the CHAMP RO profiles over the North American domain during January 2003.

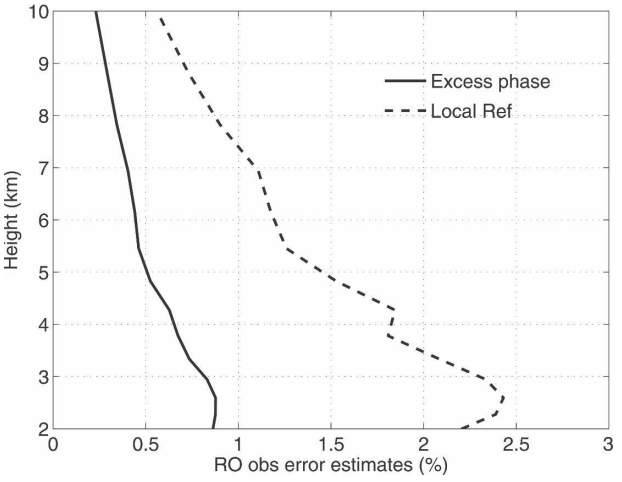

FIG. 2. CHAMP RO observation standard deviation of error estimates for excess phase (solid line) and refractivity (dashed line).

- Experiment V: Assimilate the same set of radiosonde observations as in experiment IV plus RO refractivity using the nonlocal operator.
- Experiment VI: Same as experiment V but assimilate the RO refractivity using the local refractivity operator.

The assimilation experiments are done over a North American domain where radiosondes are dense and many nearby radiosondes are available for verification of the analyses of temperature and water vapor. We examine the impact of the CHAMP RO refractivity on WRF analyses at 50-km horizontal resolution during January 2003.

5. The observations

The radiosonde observations and their error estimates are obtained from the National Centers for Environmental Prediction (NCEP) operational dataset for its global and regional data assimilation systems. The radiosondes are mainly available at 0000 and 1200 UTC.

The satellite cloud drift wind observations are obtained from the National Environmental Satellite, Data, and Information Service (NESDIS) and are thinned by using only 1 of every 20 raw observations. After thinning, there are ~3500 satellite wind observations available within the domain daily. The observation error estimates for the satellite cloud drift winds used in the NCEP operational data assimilation system are used here; the errors are significantly larger than those for the radiosonde winds.

In January 2003, there are 536 CHAMP RO profiles available over the North American domain (see Fig. 1). In each assimilation window of 6 h, there are about 17 profiles over the domain. Only the RO observations that passed the Constellation Observing System for Meteorology, Ionosphere, and Climate (COSMIC) Data Analysis and Archive Center (CDAAC) quality control (Kuo et al. 2004; Rocken et al. 2000) are used; no additional quality control is applied to the RO observations. The few RO refractivity observations below 2 km are excluded to avoid relatively larger measurement errors due to the possible existence of superreflection in the lower troposphere (see, e.g., Sokolovskiy 2003).

To reduce possible errors associated with aliasing of small-scale structures of RO refractivity onto larger-scale vertical structures of WRF model refractivity, the high-vertical-resolution raw RO data are (boxcar) averaged to the domain-averaged WRF model vertical levels. The average is done with all of the refractivity observations that are located between the interfaces of these model levels. There are nine model levels or refractivity/excess phase values in the troposphere between 2 and 10 km per profile. These observations are then assimilated using the nonlocal and local operators.

Observational error estimates for the CHAMP RO refractivity and excess phase are shown in Fig. 2. The estimates were obtained for August 2003 using a 45-km-resolution version of WRF 24-h forecasts and the

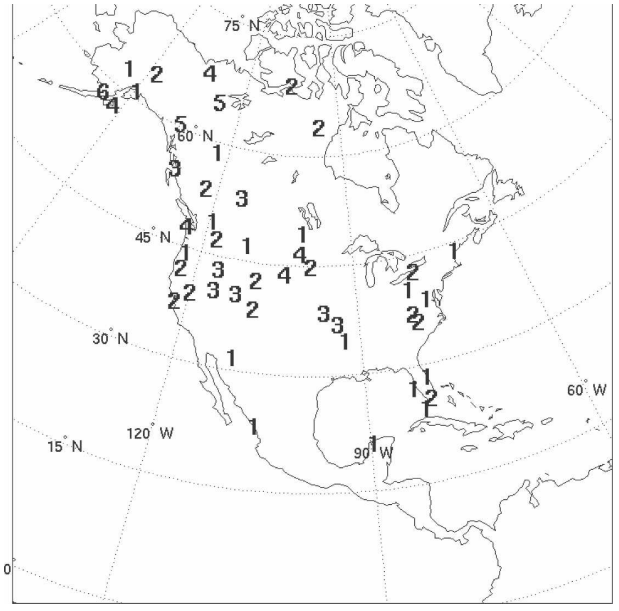

FIG. 3. Locations of the radiosonde profiles that are within 200 km and ±3 h of RO observations during January 2003; the number indicates the number of times that a radiosonde at this location was used for verification of the analyses from the assimilation experiments.

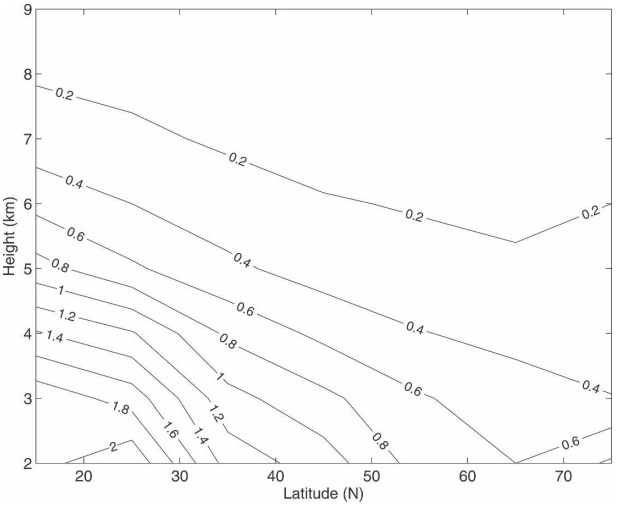

FIG. 4. Latitudinal and height distribution of the refractivity gradient [N-units (50 km)$^{-1}$] of the 6-h forecasts (ensemble mean) for experiment I at the perigee points of the CHAMP RO locations, averaged over the North American domain for January 2003.

CHAMP RO data using the Hollingsworth and Lonnberg (1986) method. The estimates include measurement and forward modeling error for WRF forecasts at 45-km resolution.

To evaluate the analyses of the assimilation experiments, radiosondes within 200 km and ±3 h of the RO observations are withheld in the assimilation experiments. A total of 104 collocated radiosondes are available during the period, and these are distributed across the North American domain (Fig. 3).

In the experiments, the RO refractivity and satellite wind observations are assimilated at 0000, 0600, 1200, and 1800 UTC and the radiosonde observations are assimilated at 0000 and 1200 UTC. The initial and boundary ensemble mean conditions are obtained from the 1 × 1 degree Aviation (AVN) analysis, produced routinely by NCEP as part of the operational weather prediction enterprise. A total of 20 ensemble members are used in this study. The initial (1 January 2003) and boundary ensembles are generated randomly according to the forecast error covariance statistics of the WRF three-dimensional variational data assimilation system (3DVAR). An alternative way to generate the initial and boundary ensembles would be to use global ensemble forecasts, but that is not done here. Since we excluded the few RO measurements below 2 km, we only examine the impact of the RO refractivity on the analyses above 800 hPa.

6. Latitudinal distribution of refractivity gradient of the first guess

In this section, we examine the refractivity gradient of the WRF 6-h forecasts in the troposphere. The magnitude of the horizontal gradient of refractivity at any observation perigee is defined as follows. First, the horizontal gradients of refractivity at the two sides of the perigee along the observed ray direction—that is, the differences between the refractivity at the perigee and the two points that are 50 km away from the perigee along the two opposite directions of the ray—are calculated. Then, the magnitudes of the two refractivity gradients are averaged to represent the magnitude of the gradient of refractivity at the perigee. Figure 4 shows the latitudinal and height distribution of the magnitude of the refractivity gradient of the 6-h forecast (ensemble mean) of experiment I, which is a composite at all RO refractivity locations over the domain during January 2003. The major feature is that the magnitude of the refractivity gradient is much larger in the lower and middle troposphere and at the low and middle latitudes. For example, a maximum of the gradient of 2 N-units (50 km)$^{-1}$ is located at 25°N near 2 km. The gradient is much weaker at 60°N near 2 km, only ~0.6 N-units (50 km)$^{-1}$.

A similar latitudinal distribution of the horizontal gradient of refractivity can also be found in the forecasts of experiment IV (Fig. 5). The gradient in experiment IV is sharper than the one in experiment I between 2 and 4 km in altitude. These distributions of the

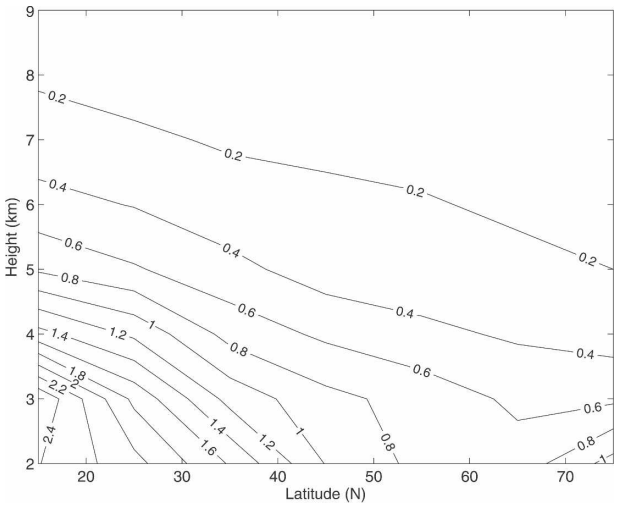

FIG. 5. Same as in Fig. 4 but for experiment IV.

refractivity gradient suggest that the use of the nonlocal operator in the assimilation of RO data may be most important in the middle and lower troposphere and at the low and middle latitudes. It is noted that the number of radio occultation observations is less in the lower troposphere and at low latitudes and so the results shown in Figs. 4 and 5 rely on a different sample size.

In the following, we will evaluate the performance of the nonlocal operator in two separate latitude belts from 15°–45°N and 45°–75°N.

7. Departures of first guess from observations

In this section, we examine the departures of the first guess from observations using the nonlocal operator and local operator. Figure 6 shows the percentage bias and RMS error relative to the observations of experiment I in the latitudes of 15°–45°N (two outlier radiosonde profiles were removed from the statistics). It can be seen that the bias and RMS error of the quasi phase in the first guess are much smaller than the refractivity calculated using the local operator. In the high latitudes of 45°–75°N, the bias and RMS error of the quasi phase is also smaller than the refractivity calculated using the local operator (Fig. 7). For experiment IV, similar results can also be found with a better fit to GPS RO observations (see Figs. 8 and 9), which suggests that experiment IV contains smaller forecast errors than experiment I.

These results suggest that use of the nonlocal operator may have significantly smaller bias and RMS error between the first guess and the observations. There-

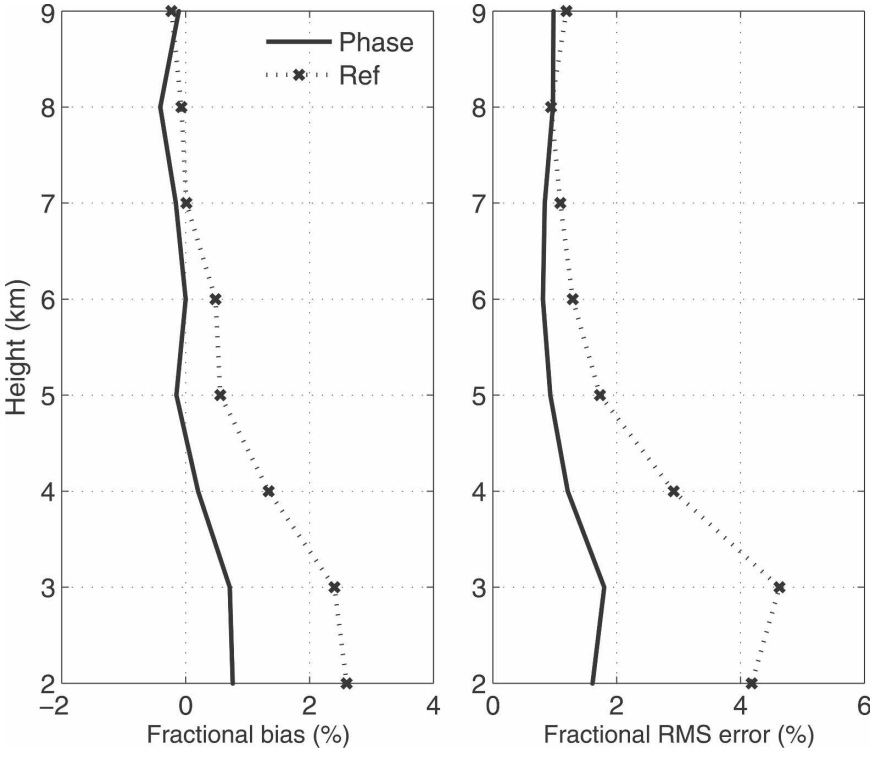

FIG. 6. (left) The percentage bias and (right) RMS departures of the nonlocal quasi-phase (solid line) and the local refractivity (dotted line) of the first guess/forecasts of experiment I from the corresponding observations averaged for the latitudes of 15°–45°N.

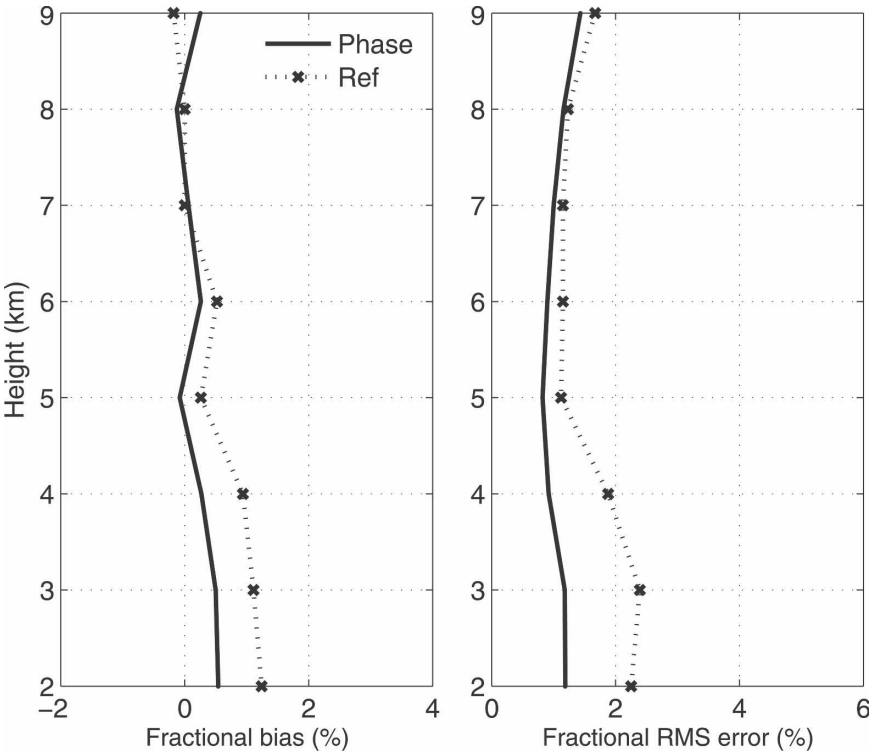

FIG. 7. Same as in Fig. 6 but for the latitudes of 45°–75°N.

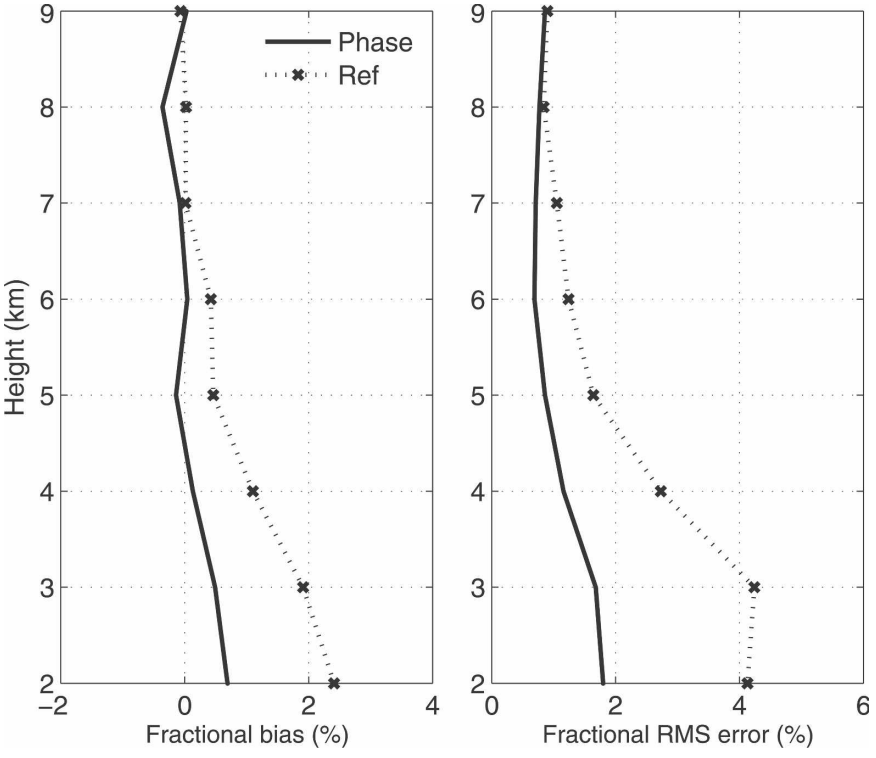

FIG. 8. Same as in Fig. 6 but for experiment IV.

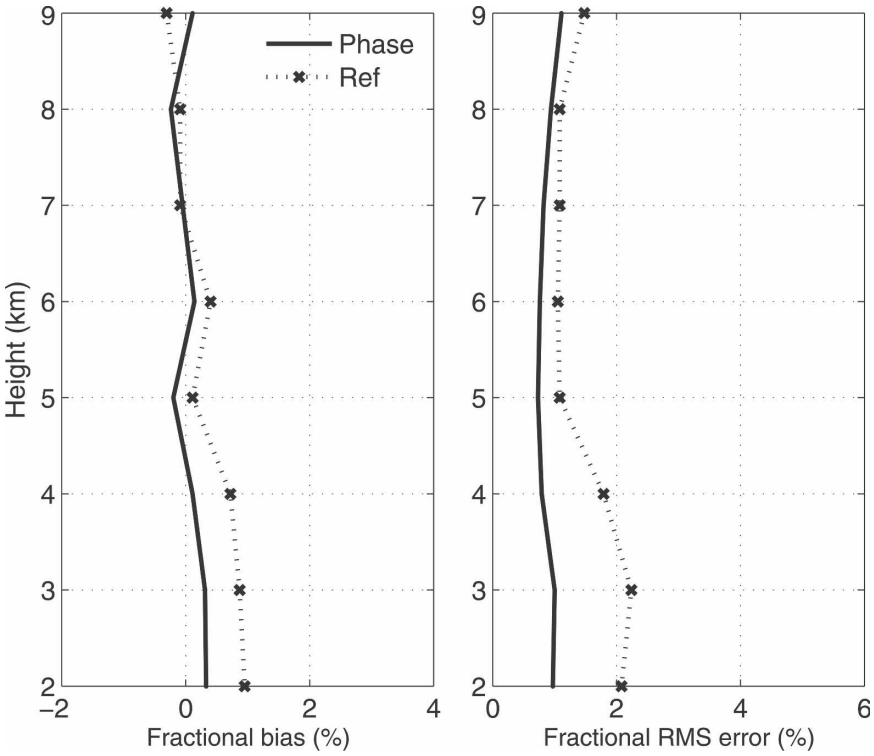

FIG. 9. Same as in Fig. 7 but for experiment IV.

fore, the use of the nonlocal operator may be able to improve the assimilation of the refractivity, as shown in the next sections, because most data assimilation systems assume zero bias of the first guess from observations. It is noted that the smaller bias and RMS error of the quasi phase does not indicate that the excess phase has more useful information than refractivity.

8. Impact of the nonlocal operator in the presence of only satellite winds

Figure 10 shows the vertical distribution of the mean and RMS fit of the analysis of temperature to the collocated radiosondes in experiments I, II, and III, averaged for the latitudes of 15°–45°N. A large cold bias of ~ -1.1 K exists at ~700 and 400 hPa in the analysis using satellite winds only. When the RO refractivity observations are assimilated using the nonlocal operator (experiment II), the cold bias is reduced to -0.75 and -0.85 K, respectively. When the RO refractivity is assimilated using the local operator, the reduction of the cold bias is not seen. The RMS error for the analysis assimilating only satellite winds has a minimum of ~2.1 K in the middle troposphere. The RO refractivity assimilated using the nonlocal operator reduces the error to ~1.5 K. When the local refractivity operator is used (experiment III), however, the reduction is only ~0.25 K, less than half of that for the nonlocal operator.

The vertical distribution of the mean and RMS fit of the analysis of specific humidity is shown in Fig. 11. The specific humidity analysis from assimilating only satellite winds has a wet bias in the lower troposphere. The RO refractivity assimilated using either the nonlocal or local operators is able to reduce the wet bias by almost half. The difference between using the nonlocal and local operator is generally small.

For the high latitudes of 45°–75°N, the vertical distributions of the mean and RMS fit of the analysis of temperature are shown in Fig. 12. The relative benefits of using the nonlocal operator are less evident because the horizontal variations of the refractivity of the forecast are much weaker than at the lower latitudes (see Figs. 4 and 5). The analysis of temperature using satellite winds has a cold bias of 0.5 K at 600 hPa. The assimilation of the RO refractivity using both the nonlocal and local operators reduces the bias. At 800 hPa, the assimilation of the RO refractivity using the nonlocal operator slightly reduces the bias, but the one using the local operator increases the bias below 700 hPa. The assimilation of the RO refractivity in concert with satellite winds also slightly reduces the RMS error of the analysis of temperature. The performance of the

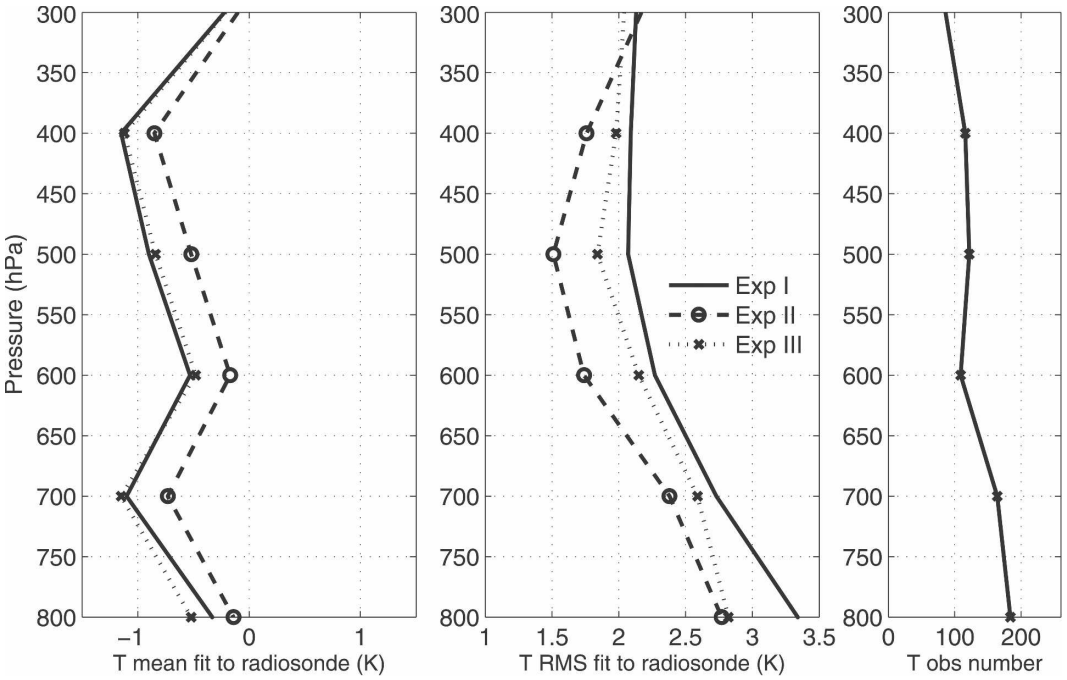

FIG. 10. Vertical distribution of (a) mean error and (b) RMS fit of temperature analysis to the collocated radiosonde temperatures, and (c) the number of verifying radiosonde temperature observations for the assimilation experiments in the presence of satellite cloud drift wind observations during January 2003. Values are averaged for the latitudes of 15°–45°N. Solid line is for assimilation of only satellite wind observations, dashed line is for the satellite wind observations plus the CHAMP RO refractivity using the nonlocal operator, and dotted line is for the satellite wind observations and the RO refractivity using the local operator.

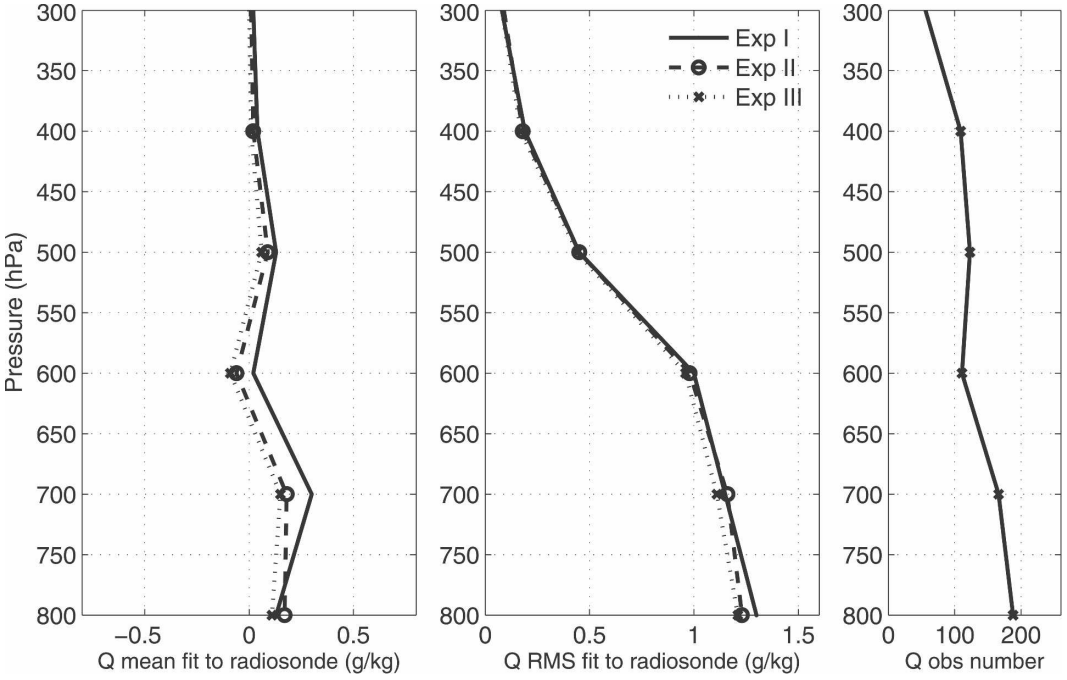

FIG. 11. Same as in Fig. 10 but for specific humidity.

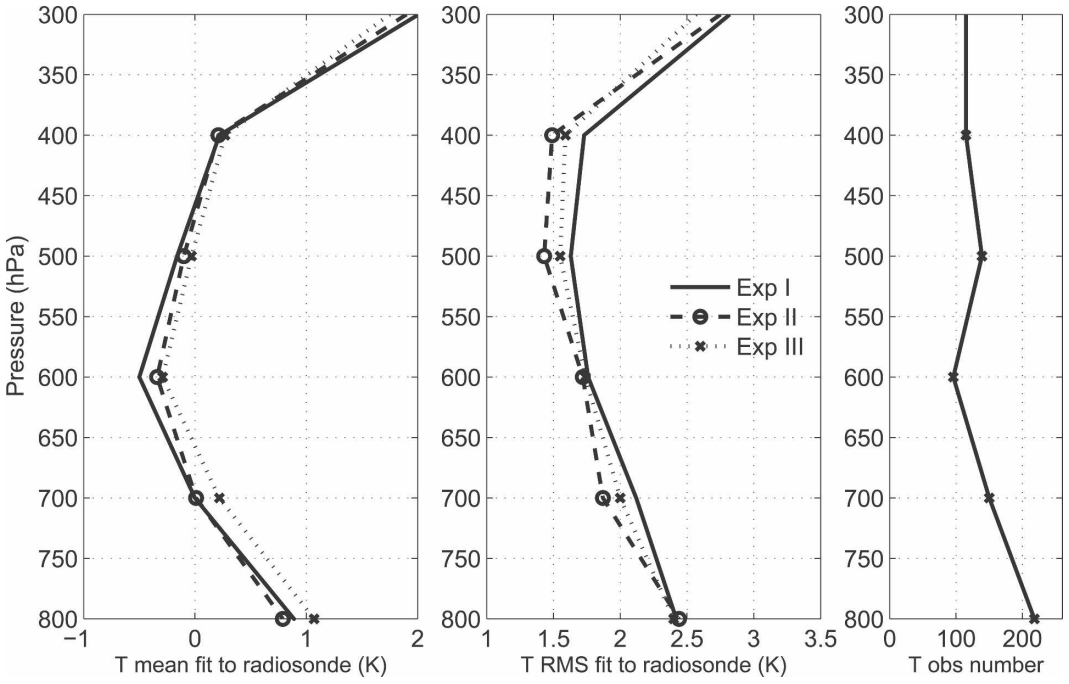

FIG. 12. Same as in Fig. 10 but for the latitudes of 45°–75°N.

nonlocal operator is slightly better than the local operator.

For specific humidity (Fig. 13), the analysis from assimilating only satellite winds has a wet bias of 0.35 g kg^{-1} at 600 hPa. The RO refractivity assimilated using both the nonlocal and local operators is able to reduce the wet bias by ~0.1 g kg^{-1}. The RO refractivity assimilated using the two operators also reduces the RMS error in the lower troposphere from 0.95 to 0.8 g kg^{-1}. The performance of the nonlocal operator is slightly better than the local operator in the lower troposphere.

9. Impact of the nonlocal operator in the presence of radiosondes

Assimilations of the radiosonde observations produce mean and RMS fits of the analysis of temperature that are significantly smaller than those from assimilating only satellite wind observations. As a result, the impact of the RO data on further improving the analyses of temperature and specific humidity is reduced in the presence of the radiosonde observations. For the latitudes of 15°–45°N, the temperature analysis assimilating radiosonde observations has a bias of only −0.5 K at 700 hPa (Fig. 14). The RO refractivity assimilated using the nonlocal operator reduces the bias to −0.4 K. The nonlocal operator performs slightly better than the local operator in the lower troposphere. In addition, the RO refractivity assimilated using the nonlocal operator reduces the RMS error of the analysis in the lower troposphere. It can be seen that use of the nonlocal operator slightly improves the analysis compared to the use of the local operator.

For specific humidity (Fig. 15), the RO refractivity assimilated using both nonlocal and local operators is able to reduce the RMS error of the analysis in the lower troposphere. The performance of the nonlocal operator is slightly better than that of the local operator. For the bias of the analysis, the RO refractivity assimilated using the local operator has no evident impact on reducing the small bias in the middle and lower troposphere. The RO refractivity assimilated using the nonlocal operator has mixed impact on the bias of the analysis in the middle and lower troposphere.

For the high latitudes of 45°–75°N, the assimilation of the RO refractivity using both the nonlocal and local operator has no noticeable impact on reducing the RMS error of the analysis of temperature in the middle and lower troposphere (Fig. 16). The assimilation of the RO refractivity using the nonlocal operator reduces slightly the bias of the analysis in the lower and middle troposphere. The assimilation of the RO refractivity using the local operator does not have noticeable impact on the bias of the analysis.

For specific humidity, the RO data modestly improve the analysis in the lower troposphere (Fig. 17). The

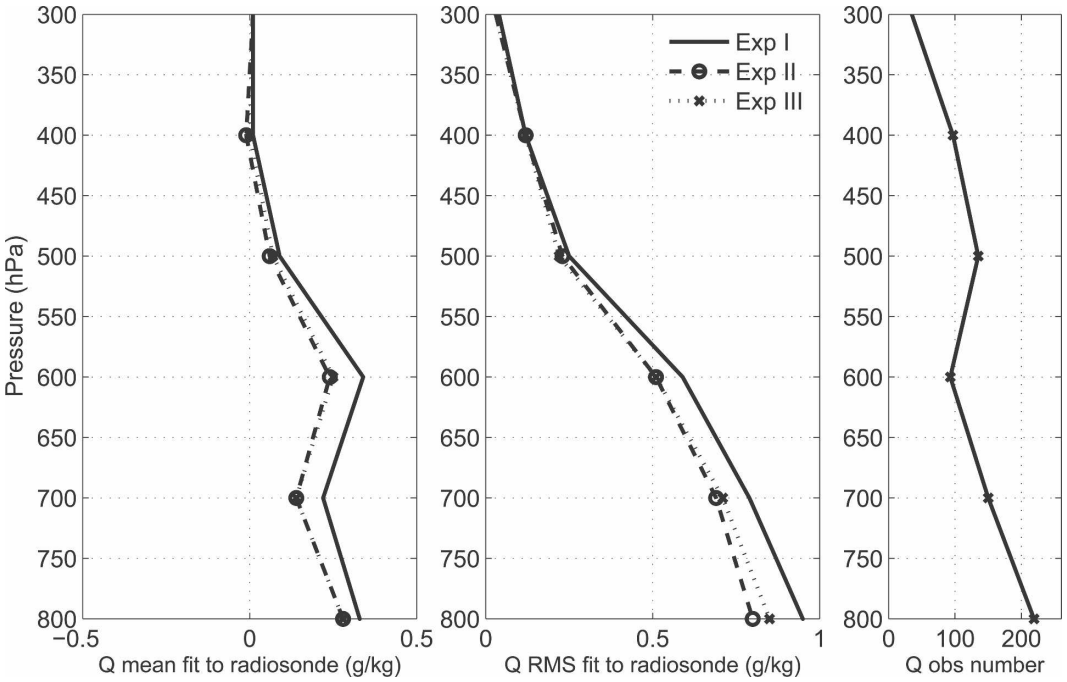

FIG. 13. Same as in Fig. 12 but for specific humidity.

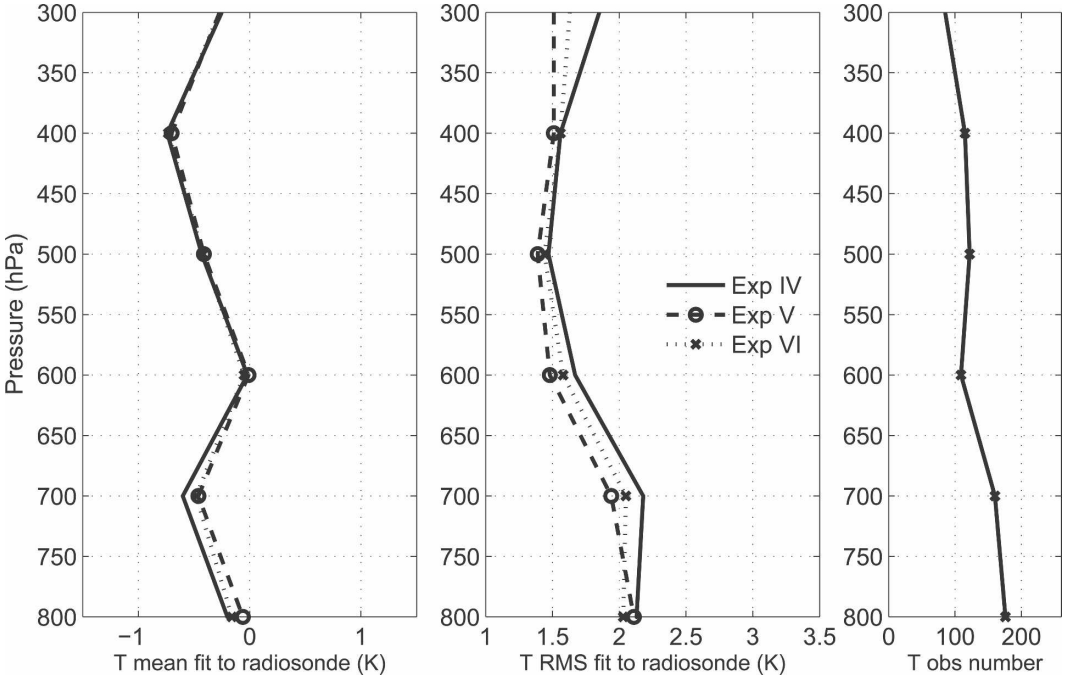

FIG. 14. Vertical distribution of (a) mean error and (b) RMS fit of temperature analysis to the withheld nearby radiosonde temperature observations, and (c) the number of the withheld radiosonde temperature observations for the assimilation experiments in the presence of radiosonde temperature, wind, and specific humidity observations during January 2003. Results are averaged over latitudes of 15°–45°N. Solid line is for assimilation of only radiosonde observations, dashed line is for radiosonde observations plus the CHAMP RO refractivity using the nonlocal operator, and dotted line is for the radiosonde observations and the RO refractivity using the local operator.

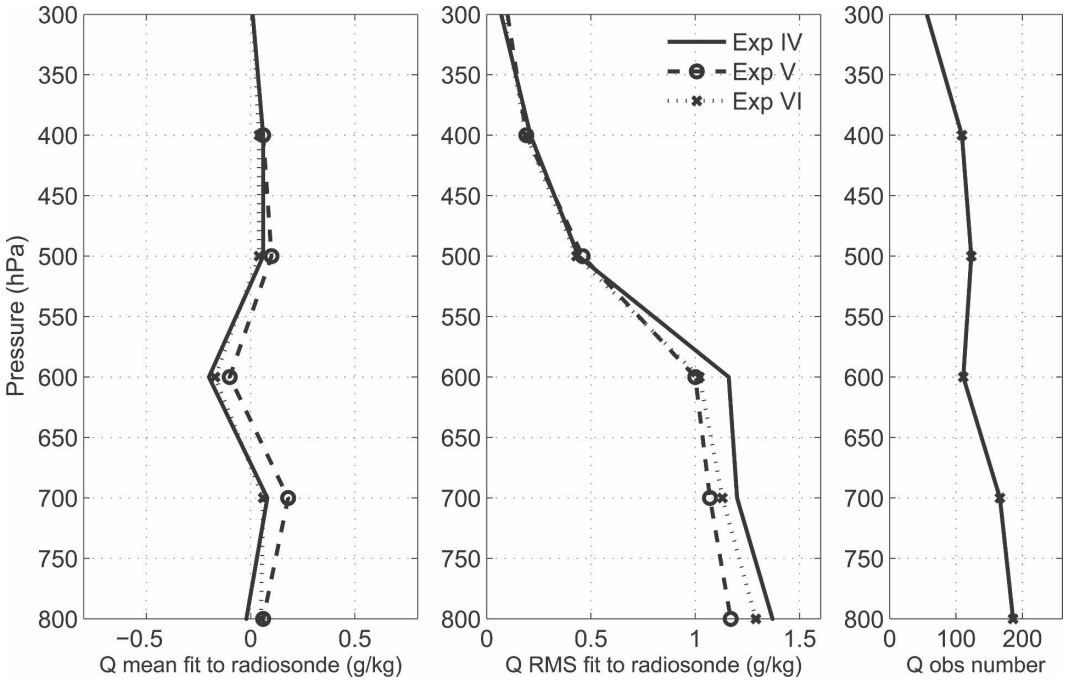

FIG. 15. Same as in Fig. 14 but for specific humidity.

analysis from assimilating radiosonde observations has a wet bias of 0.2 g kg^{-1} at 700 hPa. The RO refractivity assimilated using the nonlocal operator reduces the wet bias to ~0.1 g kg^{-1}. In addition, the RO refractivity assimilated using the nonlocal operator slightly reduces the RMS error in the lower troposphere. The performance of the nonlocal operator is slightly better than the local operator.

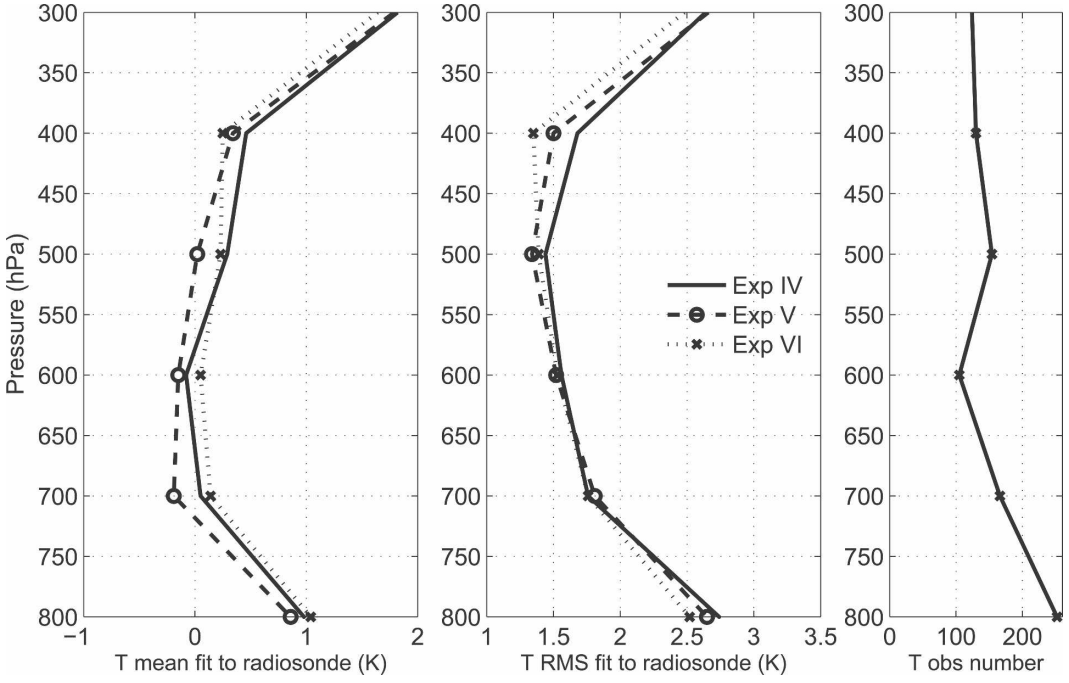

FIG. 16. Same as in Fig. 14 but for the latitudes of 45°–75°N.

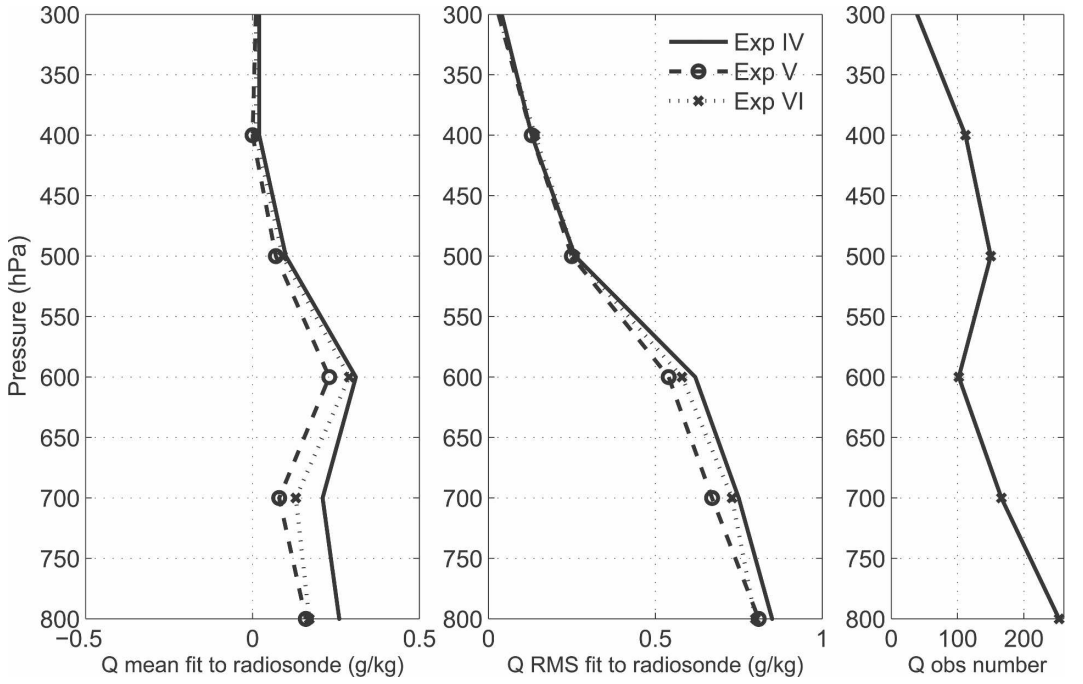

FIG. 17. Same as in Fig. 16 but for specific humidity.

10. Conclusions and discussion

In this study, a nonlocal quasi-phase operator is evaluated in assimilation of the CHAMP GPS refractivity using the WRF ensemble data assimilation system. Assimilation experiments are done over North America during January 2003 in two different situations: in conjunction with dense, high-quality radiosonde observations and with only satellite cloud drift wind observations. Analyses of temperature and specific humidity with the RO refractivity assimilated using the nonlocal operator and a local one are verified against nearby withheld radiosonde observations. It is shown that use of the nonlocal quasi-phase operator significantly reduced the bias departure of the first guess (forecasts) from the CHAMP radio occultation observations, compared with the local refractivity operator for the North America domain of January 2003. The CHAMP quasi-phase observations assimilated using the nonlocal operator reduce significantly the bias and RMS errors of WRF analyses of temperature and specific humidity in the troposphere in the presence of only satellite cloud drift wind observations. On the other hand, CHAMP refractivity assimilated using the local operator has less reduction of the errors in the analyses of temperature and specific humidity, especially in the middle and lower troposphere at the low and middle latitudes. In the presence of dense and high-quality radiosonde observations, the differences between using the local and nonlocal operators are reduced.

It may be concluded that use of the nonlocal RO quasi-phase operator can significantly improve the assimilation of RO data in the WRF ensemble assimilation system in the middle and lower troposphere, especially in regions where conventional high-quality observations are sparse and satellite winds are the major data resource. Such regions may include remote land regions, much of the extratropical oceans, and most of the tropical oceans. It should be noted, however, that the results obtained in this study might be limited to the WRF ensemble data assimilation system and may not be applicable to operational assimilation systems where many more observation types are assimilated.

We plan to further evaluate the nonlocal operator over tropical oceans where the horizontal gradient of refractivity is expected to be larger than for the middle latitudes because of the existence of abundant water vapor and small-scale convection. The WRF at a higher horizontal resolution (~30 km) will be used in the evaluation of the nonlocal operator. It is expected that the nonlocal operator may have larger advantages compared to the local operator at the higher resolution. In addition, the impact of GPS RO data on surface pressure will be examined later with COSMIC data, which penetrate much deeper into the lower troposphere.

Over tropical oceans, current global analyses of temperature and water vapor rely heavily on satellite radiances and winds. Significant areas of cloud cover may exist, especially in the vicinity of tropical storms. The satellite cloud drift and scatterometer winds may be the major data resources and the analyses of temperature and water vapor may therefore have larger uncertainty. The results obtained here suggest that GPS RO data might have potential to improve the analyses and forecasts of temperature and water vapor over the tropical oceans, especially in cloudy situations. That study is under way and will be reported separately soon.

REFERENCES

Anderson, J. L., 2001: An ensemble adjustment Kalman filter for data assimilation. *Mon. Wea. Rev.,* **129,** 2884–2903.

——, 2003: A local least squares framework for ensemble filtering. *Mon. Wea. Rev.,* **131,** 634–642.

Foelsche, U., and G. Kirchengast, 2004: Sensitivity of GNSS occultation profiles to horizontal variability in the troposphere: A simulation study. *Occultations for Probing Atmosphere and Climate,* G. Kirchengast, U. Foelsche, and A. K. Steiner, Eds., Springer-Verlag, 127–136.

Gaspari, G., and S. E. Cohn, 1999: Construction of correlation function in two and three dimensions. *Quart. J. Roy. Meteor. Soc.,* **125,** 723–757.

Healy, S. B., and J.-N. Thepaut, 2006a: Assimilation experiments with CHAMP GPS radio occultation measurements. *Quart. J. Roy. Meteor. Soc.,* **132,** 605–623.

——, J. R. Eyre, M. Hamrud, and J.-N. Thepaut, 2006b: Assimilating GPS radio occultation measurements with two-dimensional bending angle observation operators. EUMETSAT/ECMWF Fellowship Programme Research Rep. 16, 19 pp.

Hollingsworth, A., and P. Lonnberg, 1986: The statistical structure of short-range forecast errors as determined from radiosonde data. Part I: The wind field. *Tellus,* **38A,** 111–136.

Kuo, Y.-H., S. Sokolovskiy, R. Anthes, and F. Vandenberghe, 2000: Assimilation of GPS radio occultation data for numerical weather prediction. *Terr. Atmos. Oceanic Sci.,* **11,** 157–186.

——, T.-K. Wee, S. Sokolovskiy, C. Rocken, W. Schreiner, D. Hunt, and R. A. Anthes, 2004: Inversion and error estimation of GPS radio occultation data. *J. Meteor. Soc. Japan,* **82,** 507–531.

Kursinski, E. R., G. A. Hajj, K. R. Hardy, J. T. Shofield, and R. Linfied, 1997: Observing earth's atmosphere with radio occultation measurements using the Global Positioning System. *J. Geophys. Res.,* **102,** 23 429–23 465.

Liu, H., and X. Zou, 2003: Improvements to a GPS radio occultation ray-tracing model and their impacts on assimilation of bending angle. *J. Geophys. Res.,* **108,** 4548, doi:10.1029/2002JD003160.

——, J. Anderson, Y.-H. Kuo, and K. Raeder, 2007: Importance of forecast error multivariate correlations in idealized assimilations of GPS radio occultation data with the ensemble adjustment filter. *Mon. Wea. Rev.,* **135,** 173–185.

Poli, P., 2004: Effects of horizontal gradients on GPS radio occultation observation operators. II: A fast atmospheric refractivity gradient operator (FARGO). *Quart. J. Roy. Meteor. Soc.,* **130,** 2807–2825.

Rocken, C., Y.-H. Kuo, W. Schreiner, D. Hunt, S. Sokolovskiy, and C. McCormick, 2000: COSMIC system description. *Terr. Atmos. Oceanic Sci.,* **11,** 157–186.

Sokolovskiy, S., 2003: Effect of superrefraction on inversions of radio occultation signals in the lower troposphere. *Radio Sci.,* **38,** 1058, doi:10.1029/2002RS002728.

——, Y.-H. Kuo, and W. Wang, 2005a: Evaluation of a linear phase observation operator with CHAMP radio occultation data and high-resolution regional analysis. *Mon. Wea. Rev.,* **133,** 3053–3059.

——, ——, and ——, 2005b: Assessing the accuracy of a linearized observation operator for assimilation of radio occultation data: Case simulations with a high-resolution weather model. *Mon. Wea. Rev.,* **133,** 2200–2212.

Syndergaard, S., E. R. Kursinski, B. M. Herman, E. M. Lane, and D. E. Flitter, 2005: A refractive index mapping operator for assimilation of occultation data. *Mon. Wea. Rev.,* **133,** 2650–2668.

——, Y.-H. Kuo, and M. S. Lohmann, 2006: Observation operators for the assimilation of occultation data into atmospheric models: A review. *Atmosphere and Climate: Studies by Occultation Methods,* U. Foelsche, G. Kirchengast, and A. Steiner, Eds., Springer-Verlag, 205–244.

Ware, R., and Coauthors, 1996: GPS sounding of the atmosphere from low earth orbit: Preliminary results. *Bull. Amer. Meteor. Soc.,* **77,** 19–40.

Zou, X., and Coauthors, 1999: A ray-tracing operator and its adjoint for the use of GPS/MET refraction angle measurements. *J. Geophys. Res.,* **104** (D18), 22 301–22 318.